ACS OMEGA

Open Access

http://pubs.acs.org/journal/acsodf

Article

Multiomics Reveals a Mechanism: Glycogen Synthesis, Galactose Metabolism, and Ethanol Degradation Pathways, the Durable Role of Neutralizing Antibodies in Preventing COVID-19

Huayu Luo, Linrui Fan, Feng Cao, Tong Ren, Yujie He, Tao Shen, Dan Liu, and Hongzheng Ren*

Cite This: *ACS Omega* 2024, 9, 42757−42765

Read Online

ACCESS | Metrics & More | Article Recommendations

ABSTRACT: Since the emergence and rapid dissemination of Coronavirus disease 2019 (COVID-19), over 774 million individuals globally have achieved recovery to today. There is some case flashing into here and there all over the world. Neutralizing Antibody (NAb) against Severe Acute Respiratory Syndrome Coronavirus-Type 2 (SARS-CoV-2) play a paramount role in conferring effective and lasting protection for several months. This protective effect decreases with time thus increasing the chance of reinfection. Therefore, we can provide the body with a lasting protective effect by maintaining NAb level. However, how to maintain Nab level remains elusive. To address this question, we recruited 80 patients with confirmed COVID-19 and collected 480 consecutive blood samples and performed NAb testing six months after their recovery. The NAb level were categorized into two groups: a low-titer NAb group (≤20) and a high-titer NAb group (>20). To achieve a comprehensive understanding of the changes in NAb level, 16 serum samples were randomly selected for an untargeted metabolomic analysis, whereas 9 samples were designated for a label-free proteomic analysis. We successfully identified differentially expressed 751 metabolites and 845 proteins. In both the low and high NAb titer groups, we identified three key differential proteins, phosphoglucose translocase 2(PGM2), UDP-Glc 4-epimerase (GALE), and alcohol dehydrogenase 1B (ADH1B), that play important roles in fluctuating NAb level through the glycogen synthesis, galactose metabolism and ethanol degradation pathways. These three key differential proteins may serve as potential biomarkers for maintaining NAb level and enhancing immune protection in patients recovering from COVID-19.

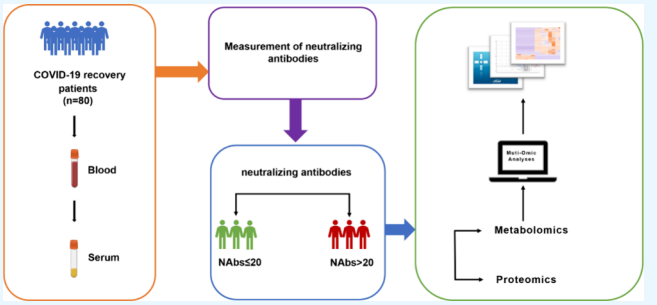

1. INTRODUCTION

Coronavirus disease 2019 (COVID-19), caused by Severe Acute Respiratory Syndrome Coronavirus Type 2 (SARS-CoV-2), was declared a global pandemic by the World Health Organization, leading to a wide range of symptoms ranging from mild to severe illness. As of 3 March, 2024 (source: https://covid19.who.int/), there have been 774 million infections and over 7 million deaths worldwide. Fortunately, COVID-19 is no longer classified as a public health emergency of international concern, though it remains a significant global health threat.[1] Progress has been made in terms of the prevention, diagnosis, and treatment of COVID-19 through mass vaccination and the implementation of various antiviral therapies.[2,3]

Currently, some research focuses on the long-term protection provided by antibodies or recovery from acute COVID-19.[4,5] Neutralizing Antibody (NAb) against SARS-CoV-2 blocks the virus's infection by targeting its structural components.[6] NAb can be acquired through vaccination or previous infections and plays a crucial role in both the treatment of SARS-CoV-2 infections and reducing the risk of reinfection.[7,8] Numerous studies found a strong correlation between NAb titer and protection against SARS-CoV-2, indicating that a decline in NAb level predicts a rapid loss of immunity that can be mitigated through booster vaccinations.[9] Once produced, NAb are expected to provide effective protection for several months.[10] But, the molecular mechanisms underlying changes of NAb titer is not clear.

Metabolomics and proteomics offer valuable tools for studying the physiological and pathological changes in body.[11,12] Changes of metabolite and protein may serve as indicators of the alteration of NAb titer. Additionally, metabolomics and proteomics can help identify potential biomarkers in the prevention and monitoring of COVID-19.

Received: April 27, 2024
Revised: September 24, 2024
Accepted: September 30, 2024
Published: October 10, 2024

2. RESULTS

2.1. Demographic and Antibody Characteristics of the Participants. In this study, we recruited 80 rehabilitated participants of COVID-19 and their six month follow up, from whom we collected demographic information and 480 serum samples in total (Table 1). The median age of the participants was 42 years, and 58.75% of them were female.

Table 1. Demographic Characteristics of the Study Population[a]

characteristics	all serum samples (n = 480)	low-titer NAb group (n = 37)	high-titer NAb group (n = 443)
Sex - no. (%)			
Male	198 (41.25%)	21 (56.75%)	177 (39.95%)
Female	282 (58.75%)	16 (43.24%)	266 (60.04%)
Age - year			
Range	23−58	31−52	23−58
Mean ± SD.	41.15 ± 9.19	42.16 ± 8.02	41.07 ± 9.23

[a]NAb, neutralizing antibody; SD, standard deviation.

As expected, we observed an overall decrease in the neutralizing antibody level over time (Figure 1). However, there were a few cases where the antibody level was ascending. Additionally, certain antibody levels remained relatively stable.

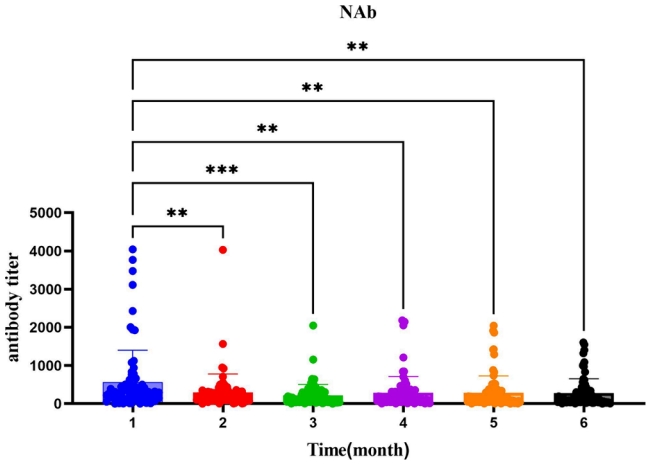

Figure 1. Neutralizing antibody level of the participants who recovered from COVID-19 during six months (** indicates p < 0.01, *** indicates p < 0.001).

2.2. Metabolic Profiles. To investigate the factors associated with the fluctuation of the NAb titer, we divided the serum samples into two groups on the basis of the level of NAb titer: the low-NAb group (≤20) and high-NAb group (>20). Subsequently, we conducted metabolomics and proteomics analysis on both groups. A random selection of 9 samples from the low-NAb group and 15 samples from the high-NAb group were subjected to metabolomic analysis. In total, 1029 metabolites with relevant information were identified across the four models. After further analysis and filtering, we ultimately detected 751 metabolites (Figure 2A), which are involved in various cellular processes, environmental information processing, and organismal systems.

PLS-DA revealed a significant difference between the low-NAb and high-NAb groups (Figure 2B). The heatmap analysis further demonstrated distinct metabolic profiles in the sera of the two NAb groups (Figure 2C). Statistical analysis of the identified metabolites revealed 34 differential metabolites, with 10 being up-regulated and 24 being down-regulated in the high-NAb group compared to the low-NAb group (Figure 2D). Through analysis using the KEGG database, we found significant enrichment in pathways such as pyruvate metabolism, the citric acid cycle, glycolysis, galactose metabolism, fructose, and mannose metabolism, as well as porphyrin and chlorophyll metabolism (Figure 2E).

Specifically, the metabolites involved in pyruvate metabolism, such as pyruvate and oxaloacetate, were significantly up-regulated in the high-NAb group. Additionally, changes were observed in other metabolites, such as those involved in porphyrin and chlorophyll metabolism, including biliverdin and bilirubin, which were significantly up-regulated in the high-NAb group.

2.3. Proteomic Profiles. To investigate the protein changes associated with NAb titer, we conducted a label-free proteomic analysis of 9 randomly selected low-NAb samples and 15 high-NAb samples. In total, we identified 55,987 unique peptides and 845 corresponding proteins across all samples. Differential analysis revealed 56 DEPs between the two groups, with 26 proteins being up-regulated and 30 proteins down-regulated in the high-NAb group (Table 2, Figure 3A). The heatmap analysis demonstrated a significant difference in the protein expression profiles between the low-NAb and high-NAb groups (Figure 3B).

Understanding the subcellular localization of proteins can provide insight into their cellular functions. Therefore, we analyzed the subcellular localization of the DEPs using the subcellular structure prediction software DeepLoc.[13] The predictions showed that the majority of proteins were located in the cytoplasm (44.64%) and nucleus (21.42%), with some proteins being extracellular (17.85%), located in the cell membrane (8.92%), or present in the endoplasmic reticulum (3.57%; Figure 3C).

Furthermore, predicting the structural domains of DEPs is essential for studying their functional regions and potential biological roles. InterProScan[14] software was used to predict the structural domains, and the top 20 proteins in the Pfam[15] database were selected for display (Figure 3D).

GO annotation provides comprehensive information about the function, localization, and biological pathways in which proteins are involved. GO function annotations are categorized into three main categories: biological process (BP), molecular function (MF), and cellular component (CC). GO analyses revealed that the DEPs were mainly enriched in megakaryocyte differentiation, protein−DNA complexes, and the structural constituent of chromatin (Figure 4A).

The pathway analysis demonstrated that the DEPs were significantly enriched in pathways such as systemic lupus erythematosus, neutrophil extracellular trap formation, and alcoholism (Figure 4B). Furthermore, the KEGG pathway enrichment analysis was performed separately for the up-regulated and down-regulated DEPs (Figure 4C).

To visualize the protein−protein interactions, we constructed protein interaction network maps based on the STRING[16] database and Cytoscape[17] software. This analysis revealed core proteins, including H4 clustered histone 6 (H4C6), phosphoglucose translocase 2(PGM2), and UDP-Glc 4-epimerase (GALE), among others (Figure 4D). Overall, the abundance of these proteins was significantly affected, indicating their potential involvement in regulating NAb.

https://doi.org/10.1021/acsomega.4c04047
ACS Omega 2024, 9, 42757−42765

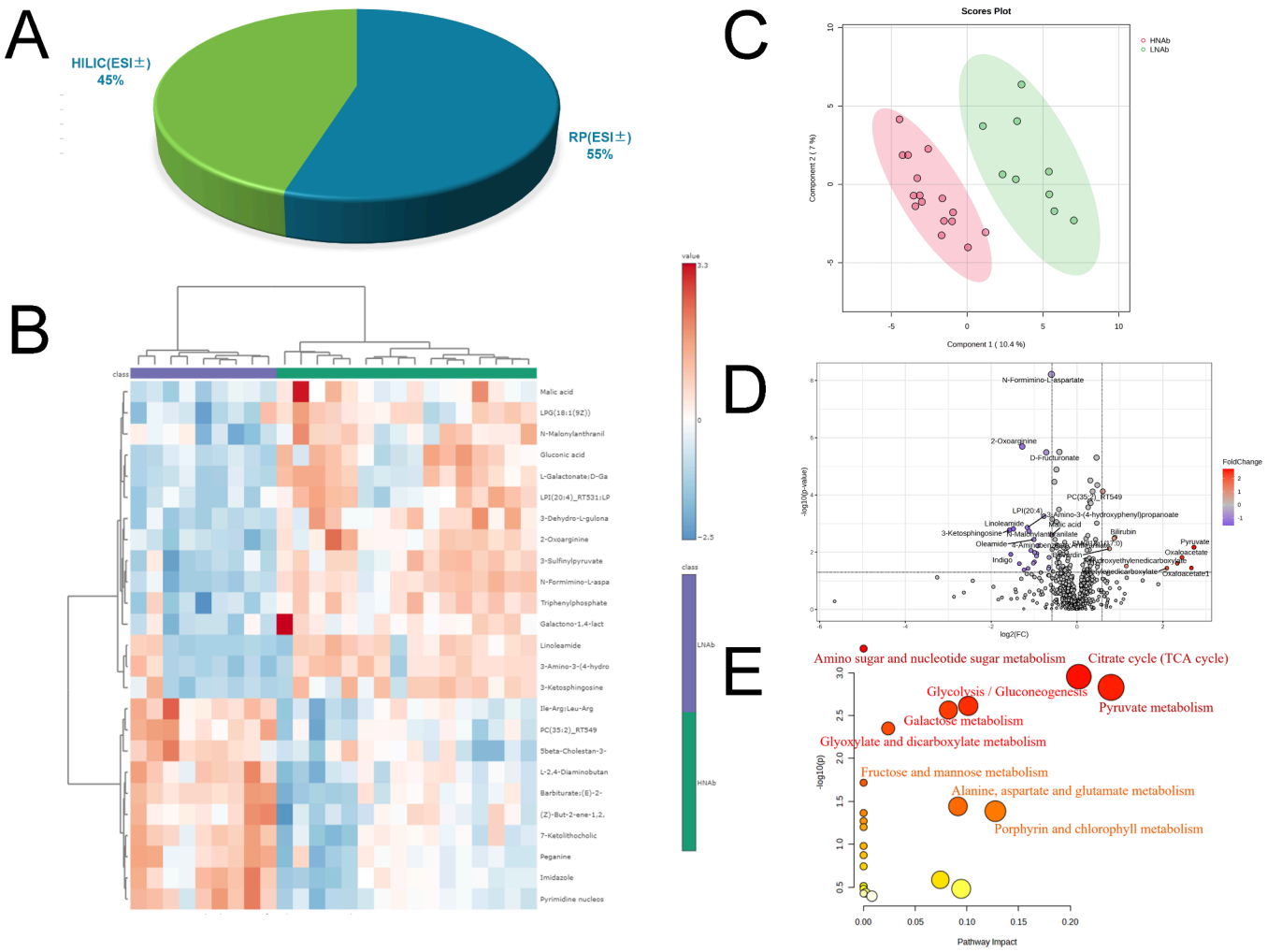

Figure 2. Metabolic changes in the low-NAb group and the high-NAb group. (A) Metabolites coidentified in the RP mode and HILIC mode. (B) Heatmap of different metabolites. Each row denotes a different metabolite, and each column denotes a sample. LNAb: low-NAb group (n = 9). HNAb: high-NAb group (n = 16). (C) Model plot of partial least-squares discriminant analysis. LNAb: low-NAb group (n = 9). HNAb: high-NAb group (n = 16). (D) Volcano plots (FC > 1.5, P < 0.05, VIP > 1). Red dots, significantly upregulated metabolites; blue dots, significantly downregulated metabolites. (E) Bubble plot of KEGG enrichment of metabolic pathways. The size of the dots denotes the number of different metabolites. Richfactor is defined as the number of differential metabolites annotated to the pathway divided by all the metabolites identified annotated to the pathway.

Table 2. Serum Antibodies of the Participants Who Recovered from COVID-19[a]

characteristics	all serum samples (n = 480)	low-titer NAb group (n = 37)	high-titer NAb group (n = 443)
NAb			
Range	0.83−4041.77	0.83−19.87	21.82−4041.77
Mean ± SD.	322.90 ± 4.99	8.31 ± 4.99	349.17 ± 526.36

[a]NAb, neutralizing antibody; SD, standard deviation.

2.4. Integrated Analysis of Metabolomic and Proteomic Data. The integration of metabolomic and proteomic data can provide valuable insights into the underlying metabolomic, and molecular mechanisms associated with physiological or pathological phenotypes.[11] In this study, we conducted a comprehensive analysis of the differentially expressed metabolites and DEPs. Through multivariate reductions in the dimensionality and visualizing the relationship of the omics data, we observed correlation between the DEPs and differential metabolites in the low-NAb group compared to the high-NAb group in COVID-19 patients during recovery (Figure 5A-B).

Enrichment analyses further revealed significant enrichment in the differentially expressed metabolites and DEPs in the galactose metabolism, amino sugar and nucleotide sugar metabolism, and glycolysis/gluconeogenesis pathways. Specifically, the metabolome predominantly involved six differential metabolites: oxalacetic acid, pyruvic acid, alpha-D-glucose, D-galactose, D-mannose, and D-fructose. Moreover, the proteome primarily included three DEPs: alcohol dehydrogenase 1B (ADH1B), GALE, and PGM2 (Figure 5C−E). Notably, most of the metabolites and proteins involved in amino sugar and nucleotide sugar metabolism and in galactose metabolism were significantly down-regulated in the high-NAb group. These findings suggest that changes in the expression levels of these metabolites and proteins may serve as markers of alterations in the level of NAb.

https://doi.org/10.1021/acsomega.4c04047
ACS Omega 2024, 9, 42757−42765

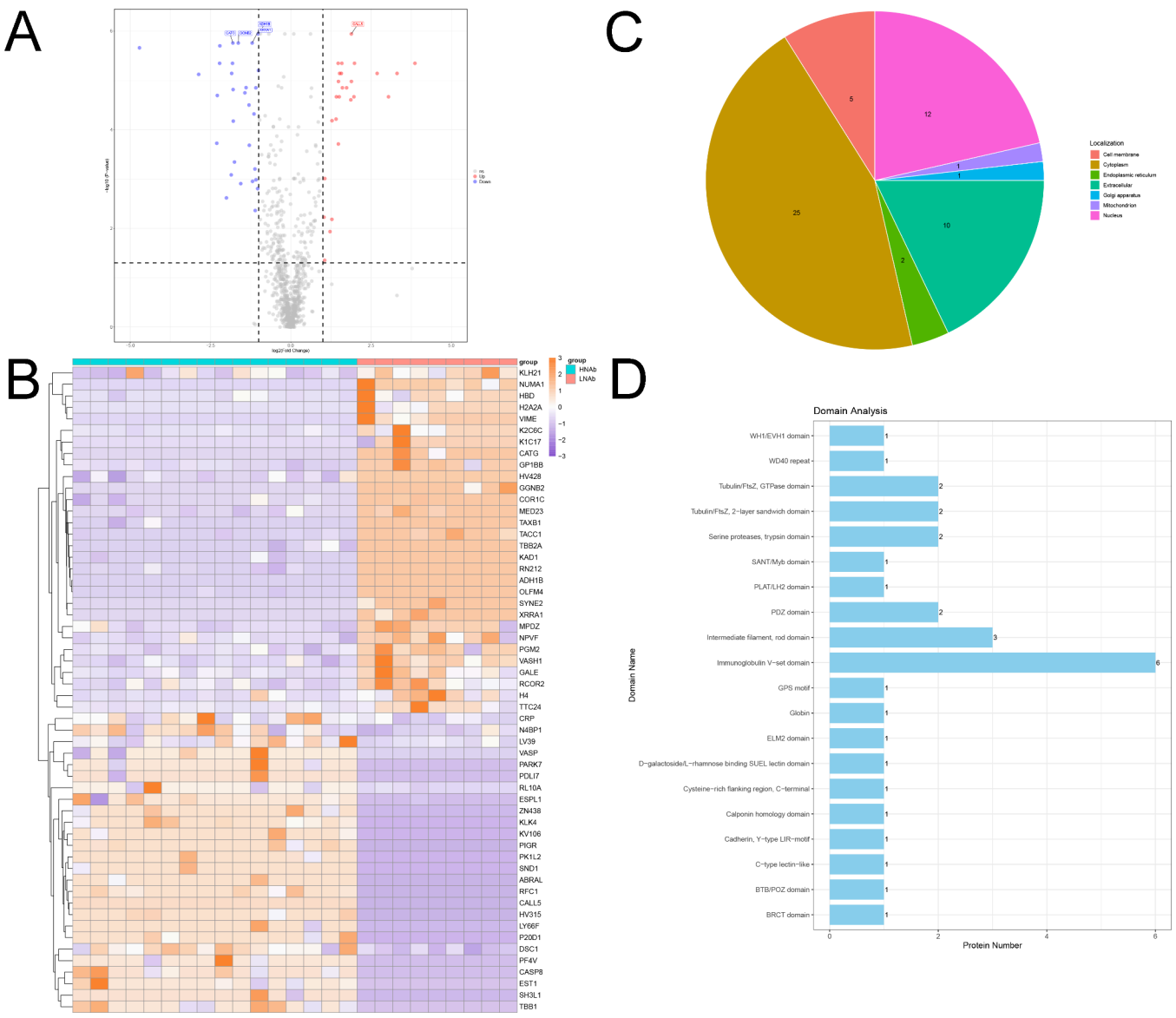

Figure 3. DEPs in the low-NAb group and the high-NAb group. (A) Volcano plots of total protein level. (B) Heatmap of different metabolites. LNAb: low-NAb group (n = 9). HNAb: high-NAb group (n = 16). (C) Map of subcellular localization of DEPs. (D) Structural domain analysis of DEPs.

3. DISCUSSION

As far as we are aware, no previous study has conducted a comprehensive multiomics investigation, at both the molecular and ionic level, to elucidate the molecular mechanisms responsible for the changes in serum NAb titer in the recovery of COVID-19 patients. This pioneering study first elucidated the serum metabolomic and proteomic profiles linked to the NAb level in recovered COVID-19 patients during the six months following up. Previous studies have demonstrated the protective effect of NAb titer against SARS-CoV-2 infection.[18,19] However, the underlying molecular mechanisms driving the changes of NAb titer remain poorly understood.

This research involved the recruited patients who had recovered from COVID-19, along with the collection of consecutive blood samples and questionnaires six months following their recovery. We measured NAb in the serum samples and observed a gradual decrease in the antibody titer over time, consistent with previous findings.[20]

In recent years, the integration of metabolomics and proteomics has emerged as a prevalent approach for identifying the biomarkers of disease[21,22] and has been extensively used to explore metabolites and proteins associated with SARS-CoV-2 infection.[15] To gain deeper insights, we utilized metabolomic and proteomic approaches to analyze the molecular pathways associated with the changes in NAb titer. In our study, we discovered significant alterations in organic acid metabolism, sugar metabolism, and porphyrin and chlorophyll metabolism related to the changes in the NAb titer. Specifically, we observed changes in proteins associated with the glycogen synthesis pathway, galactose metabolism pathway, and ethanol degradation pathway in patients during recovery from COVID-19.

In the high-titer NAb group, we observed an increase in pyruvate and oxaloacetate levels and a decrease in PGM2 and GALE, compared with the low-titer NAb group. Previous research has demonstrated that SARS-CoV-2 infection enhances glycolytic flux, leading to increased production of

https://doi.org/10.1021/acsomega.4c04047
ACS Omega 2024, 9, 42757−42765

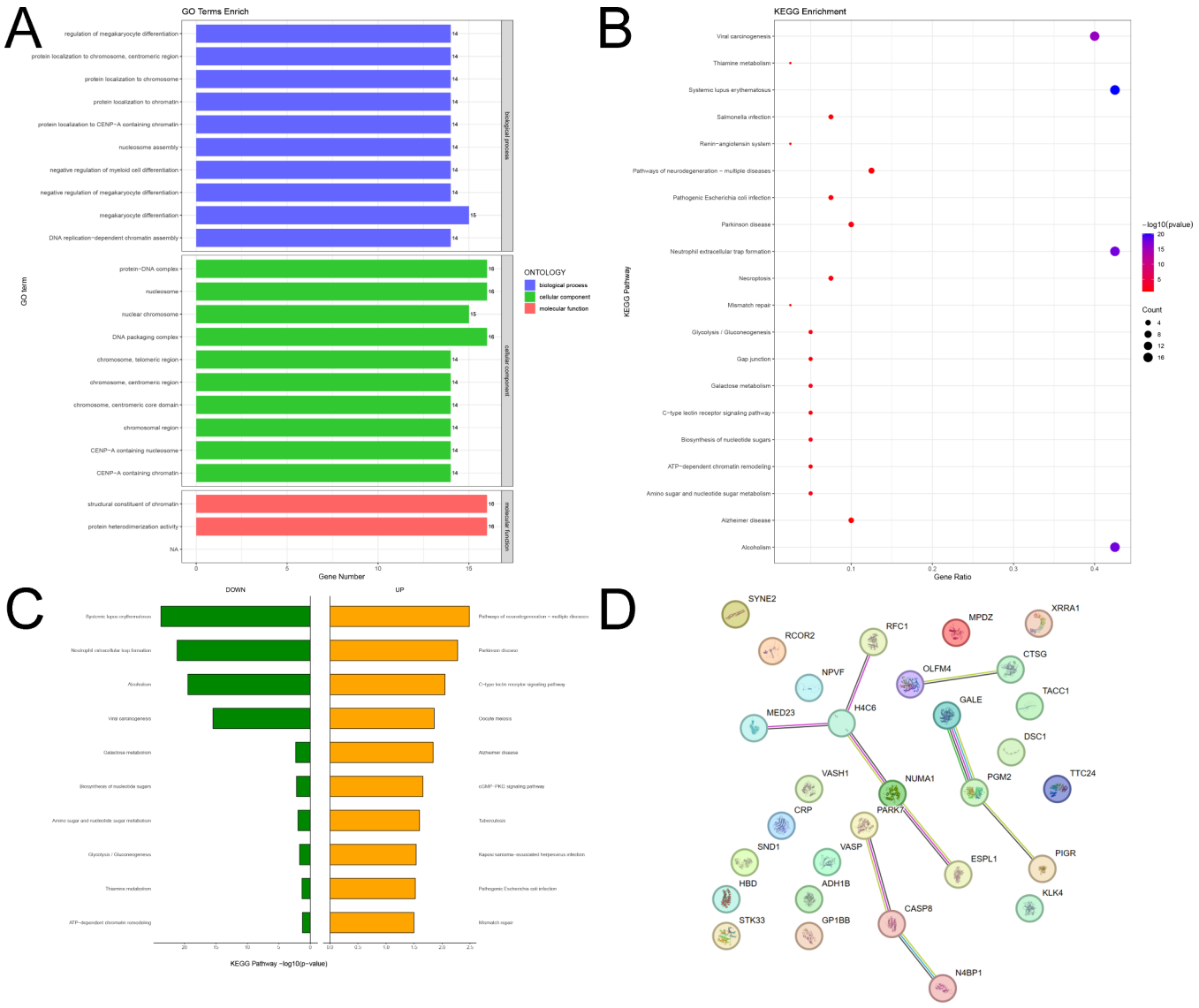

Figure 4. Protein function analysis in the low-NAb group and the high-NAb group. (A) Statistical plot of GO annotations for differential proteins. (B) Bubble plot of KEGG enrichment of metabolic pathways. (C) Butterfly map of up-regulated and down-regulated DEPs. (D) Network diagram of DEPs interactions.

lactate from pyruvate.[23] PGM2 plays a key role in the interconversion of sugar phosphates and is involved in anaerobic and catabolic reactions. In the galactose metabolic pathway, GALE catalyzes the reversible conversion of large amounts of available UDP-glucose to UDP-galactose. Moreover, glucose metabolism has been strongly correlated with COVID-19 infection.[24,25] Thus, we postulate that targeting the glycogen synthesis pathway and galactose metabolism pathway by regulating the expression of PGM2 and CALE may affect the NAb titer and the immune status of host cells.

Although a Mendelian randomization study based on UK Biobank data indicated that alcohol consumption negatively affects the progression of COVID-19 but is not associated with susceptibility to SARS-CoV-2 infection,[26] several studies have provided evidence that chronic alcohol consumption increases the risk of developing severe COVID-19.[27] Interestingly, our findings demonstrate that ADH1B, a protein associated with the ethanol degradation pathway, was significantly down-regulated in the high-NAb group. This suggests that ADH1B may play a crucial role in the prevention and prognosis of COVID-19.

Our study might be subjected to several limitations. First, the small sample sizes used for the multiomics analysis were constrained by the available resources. Second, the results obtained from the metabolomic and proteomic analysis have inherent limitations. In future studies, it will be necessary to accurately validate the identified differentially expressed metabolites and proteins to gain a deeper understanding of their underlying mechanisms.

4. CONCLUSIONS

In summary, the results of this study showed significant differences in serum metabolomic and proteomic profiles between the low and high NAb titer groups in COVID-19 infected patients six months after recovery. Multiomics analyses identified three key differential proteins, GALE, PGM2, and ADH1B, and they play important roles in the fluctuating NAb level by regulating the glycogen synthesis pathway, the galactose metabolism pathway, and the ethanol

https://doi.org/10.1021/acsomega.4c04047
ACS Omega 2024, 9, 42757−42765

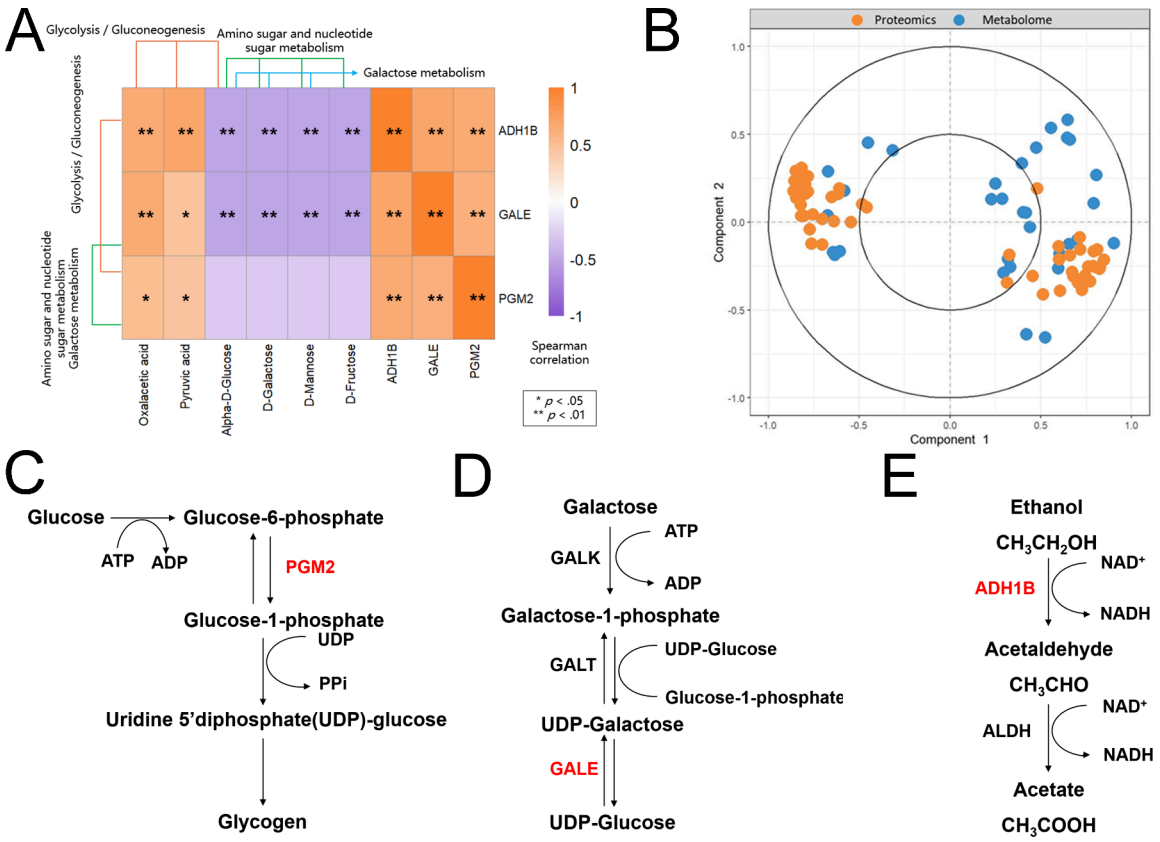

Figure 5. Proteomic and metabolomic correlation analysis of high and low NAb titers in patients recovering from COVID-19. (A) Heatmap of correlation between differential metabolites and proteins, where * indicates a correlation *P*-value of less than 0.05 and ** indicates a correlation *P*-value of less than 0.01. (B) Concentric circles of correlation between the differentially expressed metabolites and proteins. Orange dots represent differentially expressed proteins (n = 56), and blue dots represent differentially expressed metabolites (n = 34). If the angle between a differential protein and differential metabolite is an acute angle (less than 90 deg), the correlation is positive. If the angle between the differential protein and the differential metabolite is an oblique angle (greater than 90 deg and less than 180 deg), the correlation is negative. Starting from the center of the circle, the lines are connected to the differentially expressed metabolites and proteins. The longer the length of the connection, the stronger the relationship. (C) Glycogen synthesis pathway. (D) Galactose metabolism pathway. (E) Ethanol degradation pathway.

degradation pathway, respectively. These three key differential proteins may serve as potential biomarkers for the maintenance of the NAb level, thereby enhancing the effective and long-lasting protection of NAb and decreasing the rate of reinfection in COVID-19 recovered patients. These multiomics analyses present novel avenues for immune assessment and immuno-protection in patients recovering from COVID-19, providing valuable insights for the development of new strategies to maintain antibody-mediated protection.

5. MATERIALS AND METHODS

5.1. Ethical Statement. Written informed consent was obtained from all participants, and the study protocols were approved by the Institutional Review Boards of Gongli Hospital.

5.2. Patient Recruitment and Sample Collection. In total, 80 participants of COVID-19 were recruited from the community. These participants had a confirmed history of COVID-19 based on previous reverse transcription-polymerase chain reaction (RT-PCR) tests and were all infected by December 2022. During the 1−6 month follow-up period after recovery, the participants provided 5 mL of venous blood and completed a questionnaire regarding the age, the date of positive PCR results for COVID-19, their symptoms, and their vaccination status.

All selected participants complied with a strict fasting period of 12 h and were prohibited from taking medications within 48 h prior to blood sample collection. Five mL of venous blood was collected, and serum was obtained through centrifugation at 4 °C (2000 rpm, 10 min). Each serum sample was divided into four aliquots, with two used for analysis of serum NAb, and the remaining were used for metabolomic and proteomic analysis.

5.3. Quantification of NAb. The quantification of SARS-CoV-2 NAb in serum samples was performed using a pseudovirus-based virus neutralization test (Tecan, Shanghai, SparkCyto). The tests were carried out by the instruction of the reagent kits.

5.4. Metabolic Analysis. Total 25 serum samples were randomly selected for metabolomic analysis, including 9 samples from the group with low NAb titer (≤20) and 16 samples from the group with high NAb titer (>20).

The metabolites in the serum samples were extracted using a mixture of methanol and acetonitrile in a ratio of 1:1. To ensure the repeatability and stability of the liquid chromatography (LC)-mass spectrometry (MS) analysis process, 10 μL of the supernatant was taken from each of the 25 processed samples to prepare the quality control samples. The quality control samples were then evenly inserted throughout the analysis runs to monitor the stability of the large-scale analysis.

https://doi.org/10.1021/acsomega.4c04047
ACS Omega 2024, 9, 42757−42765

Furthermore, each processed sample was divided into four fractions. Two fractions were used for reverse-phase/ultra-performance liquid chromatography (RP) UPLC-MS/MS methods with positive/negative-ion mode electrospray ionization (ESI). The remaining were used for hydrophilic interaction liquid chromatography (HILIC)UPLC-MS/MS methods with ESI in positive-ion mode and negative-ion mode.

5.4.1. Conditions of Liquid Chromatography. The LC analysis was conducted by using an Exion LC 30AD System (SCIEX, MA, USA). Chromatography was performed with an ACQUITY UPLC HSS T3 column (2.1 × 100 mm, 1.8 μm) (Waters, Milford, MA, USA) and an ACQUITY UPLC BEH Amide column (2.1 × 100 mm, 3.0 μm) (Waters, Milford, MA, USA), which were maintained at a temperature of 40 °C. The flow rate was set at 0.3 mL/min, and the injection volume was 2 μL.

For the (RP)UPLC-MS/MS mode, the mobile phases consisted of (B1) 0.1% formic acid in methanol:acetonitrile (50:50, v/v) and (A1) 0.1% formic acid in water. The separation was carried out using the following gradient: 0−1.8 min, 3% B1; 1.8−11 min, 3%−95% B1; 11−16 min, 95% B1; 16−16.1 min, 95%−3% B1; 16.1−20 min, 3% B1.

For the (HILIC)UPLC-MS/MS mode, the analytes were carried out with (B2) 10 mM ammonium format in acetonitrile:water (95:5, v/v) and (A2) 10 mM ammonium format in water. The separation was conducted using the following gradient: 0−1 min, 95% B2; 1−10 min, 95%−75% B2; 10−13 min, 75%−40% B2; 13−16 min, 40% B2; 16−16.1 min, 40%−95% B2; 16.1−20 min, 95% B2.

5.4.2. Conditions of Mass Spectrometry. The detection of metabolites by MS was performed using a ZenoTOF 7600 system (SCIEX, MA, USA) equipped with an ESI ion source. The full-scan mode was applied with a scan range of 50−1300 m/z. During data collection, mass axis calibration and blank determination were performed every five injections to track the stability and background value of the instrument.

5.4.3. Metabolite Matching and Statistical Analysis. Raw data were acquired and pretreated using SCIEX OS v2.1.6 software. The data file (.wiff) was converted into mzXML and MGF formats by using MSConvert. Peaks were extracted using the XCMS package in R. The output file contained sample names, m/z pairs, retention times, and peak intensity. The MS/MS data were further processed for metabolite identification by using MetDNA2 (http://metdna.zhulab.cn/). The molecular weight tolerances were set to ±10 ppm, relative to the theoretical value for each standard metabolite.

The statistical analysis was conducted using MetaboAnalyst 5.0 (http://www.metaboanalyst.ca). The group comparisons were performed using t test. A P-value less than 0.05 was considered statistically significant. The method stability of metabolomic analysis was confirmed by evaluating the principal component analysis (PCA) score plot. The partial least-squares discriminant analysis (PLS-DA) models were established to distinguish the metabolite characteristics of two groups. Metabolic features that differentiated the low NAb group from the high NAb group were identified based on a variable importance in the projection (VIP) value greater than 1.0 in the PLS-DA, peak intensities between two groups with a P-value <0.05 and Metabolites with fold changes greater than or equal to 1.5. The obtained results were then integrated with the KEGG database and the Human Metabolome Database (HMDB) to investigate metabolic pathways and disease information related to differential metabolites.

5.5. Proteomic Analysis. Twenty-five serum samples, the same as the metabolic analysis, were used for this test. We combined BioRAD ProteoMiner beads with the serum samples in a 1.5 mL centrifuge tube and mixed them on a vertical rotating mixer for 2 h. The mixture was then centrifuged at 10000g for 5 min at 4 °C, and the beads were repeatedly washed with a wash buffer. After washing, we added 0.4 mL of 1% TFA to the beads and mixed them for 10 min. We collected the supernatant and repeated the elution process twice. The supernatant was subsequently frozen and dried into a powder using a freeze concentrator. The pellet was dissolved using a dissolution buffer (8 M urea, 100 mM TEAB, pH 8.5).

Next, the protein sample was reduced with 10 mM DTT at 56 °C for 1 h, followed by alkylation with iodoacetamide in the dark at room temperature for 1 h. The quality of the protein sample was evaluated. Then, we added DB protein lysate, trypsin, and 100 mM TEAB buffer to the protein sample, mixed well, and digested it at 37 °C for 4 h. Overnight digestion was carried out by adding trypsin and $CaCl_2$. After adjusting the pH and centrifuging for 5 min, we collected the supernatant and passed it slowly through a ^{18}C desalting column. The column was washed three times with 0.1% formic acid and 3% acetonitrile. Finally, we added an appropriate amount of eluent, collected the filtrate, and freeze-dried it.

5.5.1. Database Search for Quantification. For proteomics data analysis, MS raw data were searched using Proteome Discoverer (Version 2.4.1.15, Thermo Fisher Scientific) against a manually annotated and reviewed *Homo sapiens* protein FASTA database (SwissProt, 27 April 27, 2020). The enzyme digestion was set to fully specific trypsin, with up to two missed cleavages. Static modifications included carbamidomethylation of cysteine. Variable modifications included the oxidation of methionine and the acetylation of N-terminus peptides. The precursor ion mass tolerance was set to 10 ppm, and the product ion tolerance was set to 0.02 Da. The peptide-spectrum match allowed a 1% target false discovery rate (FDR). The protein abundance ratios of the target samples compared with the pooled sample within each batch were used as the relative protein abundance for data analysis.

5.5.2. Statistical and Bioinformatics Analysis. Statistical analysis of the protein quantification results was performed using the t test. Proteins that showed a significant difference in quantification between the experimental group and the control group ($p < 0.05$, $|\log^2 FC| > *$ ($FC > *$ or $FC < *$ [fold change, FC]) were identified as differentially expressed proteins (DEPs).

Functional annotation of serological proteins employed the PANTHER database (http://pantherdb.org/). The interaction network analysis of biological processes and signaling pathways used Cytoscape and ClueGO with a P-value cutoff ≤ 0.01. Pathway analysis employed the KEGG database (https://www.genome.jp/kegg/).

AUTHOR INFORMATION

Corresponding Author

Hongzheng Ren − *Department of Pathology, Gongli Hospital of Shanghai Pudong New Area, Shanghai 200135, China;* orcid.org/0009-0005-0241-0067; Email: rhz01672@glhospital.com

Authors

Huayu Luo − *Department of Pathology, Gongli Hospital of Shanghai Pudong New Area, Shanghai 200135, China;*

https://doi.org/10.1021/acsomega.4c04047
ACS Omega 2024, 9, 42757−42765

Department of Pathology, Changzhi Medical College Affiliated Heping Hospital, Changzhi, Shanxi Province 046000, China

Linrui Fan − *Department of Prevention & Healthcare, Gongli Hospital of Shanghai Pudong New Area, Shanghai 200135, China*

Feng Cao − *Department of Prevention & Healthcare, Gongli Hospital of Shanghai Pudong New Area, Shanghai 200135, China*

Tong Ren − *School of Nursing, Peking Union Medical College, Beijing 100144, China*

Yujie He − *Department of Pathology, Gongli Hospital of Shanghai Pudong New Area, Shanghai 200135, China*

Tao Shen − *Department of Pathology, Gongli Hospital of Shanghai Pudong New Area, Shanghai 200135, China; Department of Pathology, Changzhi Medical College Affiliated Heping Hospital, Changzhi, Shanxi Province 046000, China*

Dan Liu − *Shanghai AB Sciex Analytical Instrument Trading Co., Ltd., Shanghai 200050, China*

Complete contact information is available at: https://pubs.acs.org/10.1021/acsomega.4c04047

Notes

The authors declare no competing financial interest.

■ ACKNOWLEDGMENTS

The study was supported by Key Important Laboratory Funding in Pudong New Area, Shanghai (PWZbr2022-18).

■ REFERENCES

(1) de Araújo, G. R.; de Castro, P.; Ávila, I. R.; Bezerra, J. M. T.; Barbosa, D. S. Effects of public health emergencies of international concern on disease control: a systematic review. *Rev. Panam Salud Publica* **2023**, *47*, No. e74.

(2) Bakadia, B. M.; He, F.; Souho, T.; Lamboni, L.; Ullah, M. W.; Boni, B. O.; Ahmed, A. A. Q.; Mukole, B. M.; Yang, G. Prevention and treatment of COVID-19: Focus on interferons, chloroquine/hydroxychloroquine, azithromycin, and vaccine. *Biomed Pharmacother* **2021**, *133*, 111008.

(3) Salian, V. S.; Wright, J. A.; Vedell, P. T.; Nair, S.; Li, C.; Kandimalla, M.; Tang, X.; Carmona Porquera, E. M.; Kalari, K. R.; Kandimalla, K. K. COVID-19 Transmission, Current Treatment, and Future Therapeutic Strategies. *Mol. Pharmaceutics* **2021**, *18* (3), 754−771.

(4) Lopez-Leon, S.; Wegman-Ostrosky, T.; Perelman, C.; Sepulveda, R.; Rebolledo, P. A.; Cuapio, A.; Villapol, S. More than 50 long-term effects of COVID-19: a systematic review and meta-analysis. *Sci. Rep.* **2021**, *11* (1), 16144.

(5) Rodriguez-Morales, A. J.; Lopez-Echeverri, M. C.; Perez-Raga, M. F.; Quintero-Romero, V.; Valencia-Gallego, V.; Galindo-Herrera, N.; López-Alzate, S.; Sánchez-Vinasco, J. D.; Gutiérrez-Vargas, J. J.; Mayta-Tristan, P.; Husni, R.; Moghnieh, R.; Stephan, J.; Faour, W.; Tawil, S.; Barakat, H.; Chaaban, T.; Megarbane, A.; Rizk, Y.; Sakr, R.; Escalera-Antezana, J. P.; Alvarado-Arnez, L. E.; Bonilla-Aldana, D. K.; Camacho-Moreno, G.; Mendoza, H.; Rodriguez-Sabogal, I. A.; Millán-Oñate, J.; Lopardo, G.; Barbosa, A. N.; Cimerman, S.; Chaves, T.; Orduna, T.; Lloveras, S.; Rodriguez-Morales, A. G.; Thormann, M.; Zambrano, P. G.; Perez, C.; Sandoval, N.; Zambrano, L.; Alvarez-Moreno, C. A.; Chacon-Cruz, E.; Villamil-Gomez, W. E.; Benites-Zapata, V.; Savio-Larriera, E.; Cardona-Ospina, J. A.; Risquez, A.; Forero-Peña, D. A.; Henao-Martínez, A. F.; Sah, R.; Barboza, J. J.; León-Figueroa, D. A.; Acosta-España, J. D.; Carrero-Gonzalez, C. M.; Al-Tawfiq, J. A.; Rabaan, A. A.; Leblebicioglu, H.; Gonzales-Zamora, J. A.; Ulloa-Gutiérrez, R. The global challenges of the long COVID-19 in adults and children. *Travel Med. Infect Dis* **2023**, *54*, 102606.

(6) Frigerio, R.; Marusic, C.; Villani, M. E.; Lico, C.; Capodicasa, C.; Andreano, E.; Paciello, I.; Rappuoli, R.; Salzano, A. M.; Scaloni, A.; Baschieri, S.; Donini, M. Production of two SARS-CoV-2 neutralizing antibodies with different potencies in Nicotiana benthamiana. *Front Plant Sci.* **2022**, *13*, 956741.

(7) Al Kaabi, N.; Zhang, Y.; Xia, S.; Yang, Y.; Al Qahtani, M. M.; Abdulrazzaq, N.; Al Nusair, M.; Hassany, M.; Jawad, J. S.; Abdalla, J.; Hussein, S. E.; Al Mazrouei, S. K.; Al Karam, M.; Li, X.; Yang, X.; Wang, W.; Lai, B.; Chen, W.; Huang, S.; Wang, Q.; Yang, T.; Liu, Y.; Ma, R.; Hussain, Z. M.; Khan, T.; Saifuddin Fasihuddin, M.; You, W.; Xie, Z.; Zhao, Y.; Jiang, Z.; Zhao, G.; Zhang, Y.; Mahmoud, S.; ElTantawy, I.; Xiao, P.; Koshy, A.; Zaher, W. A.; Wang, H.; Duan, K.; Pan, A.; Yang, X. Effect of 2 Inactivated SARS-CoV-2 Vaccines on Symptomatic COVID-19 Infection in Adults: A Randomized Clinical Trial. *Jama* **2021**, *326* (1), 35−45.

(8) Suthar, M. S.; Zimmerman, M. G.; Kauffman, R. C.; Mantus, G.; Linderman, S. L.; Hudson, W. H.; Vanderheiden, A.; Nyhoff, L.; Davis, C. W.; Adekunle, O.; Affer, M.; Sherman, M.; Reynolds, S.; Verkerke, H. P.; Alter, D. N.; Guarner, J.; Bryksin, J.; Horwath, M. C.; Arthur, C. M.; Saakadze, N.; Smith, G. H.; Edupuganti, S.; Scherer, E. M.; Hellmeister, K.; Cheng, A.; Morales, J. A.; Neish, A. S.; Stowell, S. R.; Frank, F.; Ortlund, E.; Anderson, E. J.; Menachery, V. D.; Rouphael, N.; Mehta, A. K.; Stephens, D. S.; Ahmed, R.; Roback, J. D.; Wrammert, J. Rapid Generation of Neutralizing Antibody Responses in COVID-19 Patients. *Cell Rep. Med.* **2020**, *1* (3), 100040.

(9) Cromer, D.; Steain, M.; Reynaldi, A.; Schlub, T. E.; Wheatley, A. K.; Juno, J. A.; Kent, S. J.; Triccas, J. A.; Khoury, D. S.; Davenport, M. P. Neutralising antibody titres as predictors of protection against SARS-CoV-2 variants and the impact of boosting: a meta-analysis. *Lancet Microbe* **2022**, *3* (1), e52−e61.

(10) Dan, J. M.; Mateus, J.; Kato, Y.; Hastie, K. M.; Yu, E. D.; Faliti, C. E.; Grifoni, A.; Ramirez, S. I.; Haupt, S.; Frazier, A.; Nakao, C.; Rayaprolu, V.; Rawlings, S. A.; Peters, B.; Krammer, F.; Simon, V.; Saphire, E. O.; Smith, D. M.; Weiskopf, D.; Sette, A.; Crotty, S., Immunological memory to SARS-CoV-2 assessed for up to 8 months after infection. *Science* **2021**, *371* (6529). DOI: 10.1126/science.abf4063

(11) Shen, B.; Yi, X.; Sun, Y.; Bi, X.; Du, J.; Zhang, C.; Quan, S.; Zhang, F.; Sun, R.; Qian, L.; Ge, W.; Liu, W.; Liang, S.; Chen, H.; Zhang, Y.; Li, J.; Xu, J.; He, Z.; Chen, B.; Wang, J.; Yan, H.; Zheng, Y.; Wang, D.; Zhu, J.; Kong, Z.; Kang, Z.; Liang, X.; Ding, X.; Ruan, G.; Xiang, N.; Cai, X.; Gao, H.; Li, L.; Li, S.; Xiao, Q.; Lu, T.; Zhu, Y.; Liu, H.; Chen, H.; Guo, T. Proteomic and Metabolomic Characterization of COVID-19 Patient Sera. *Cell* **2020**, *182* (1), 59−72.

(12) Bojkova, D.; Klann, K.; Koch, B.; Widera, M.; Krause, D.; Ciesek, S.; Cinatl, J.; Münch, C. Proteomics of SARS-CoV-2-infected host cells reveals therapy targets. *Nature* **2020**, *583* (7816), 469−472.

(13) Almagro Armenteros, J. J.; Sønderby, C. K.; Sønderby, S. K.; Nielsen, H.; Winther, O. DeepLoc: prediction of protein subcellular localization using deep learning. *Bioinformatics* **2017**, *33* (21), 3387−3395.

(14) Jones, P.; Binns, D.; Chang, H. Y.; Fraser, M.; Li, W.; McAnulla, C.; McWilliam, H.; Maslen, J.; Mitchell, A.; Nuka, G.; Pesseat, S.; Quinn, A. F.; Sangrador-Vegas, A.; Scheremetjew, M.; Yong, S. Y.; Lopez, R.; Hunter, S. InterProScan 5: genome-scale protein function classification. *Bioinformatics* **2014**, *30* (9), 1236−40.

(15) Finn, R. D.; Coggill, P.; Eberhardt, R. Y.; Eddy, S. R.; Mistry, J.; Mitchell, A. L.; Potter, S. C.; Punta, M.; Qureshi, M.; Sangrador-Vegas, A.; Salazar, G. A.; Tate, J.; Bateman, A. The Pfam protein families database: towards a more sustainable future. *Nucleic Acids Res.* **2016**, *44* (D1), D279−85.

(16) Tan, S.; Chao, R. An Exploration of Osteosarcoma Metastasis Diagnostic Markers Based on Tumor-Associated Neutrophils. *Discov Med.* **2023**, *35* (176), 300−311.

(17) Shannon, P.; Markiel, A.; Ozier, O.; Baliga, N. S.; Wang, J. T.; Ramage, D.; Amin, N.; Schwikowski, B.; Ideker, T. Cytoscape: a

software environment for integrated models of biomolecular interaction networks. *Genome Res.* **2003**, *13* (11), 2498−504.
(18) Li, C. J.; Chao, T. L.; Chang, T. Y.; Hsiao, C. C.; Lu, D. C.; Chiang, Y. W.; Lai, G. C.; Tsai, Y. M.; Fang, J. T.; Ieong, S.; Wang, J. T.; Chang, S. Y.; Chang, S. C. Neutralizing Monoclonal Antibodies Inhibit SARS-CoV-2 Infection through Blocking Membrane Fusion. *Microbiol Spectr* **2022**, *10* (2), No. e0181421.
(19) Iwamoto, C.; Lesteberg, K. E.; Lamb, M. M.; Calvimontes, D. M.; Guo, K.; Barrett, B. S.; Mickens, K. L.; Duca, L. M.; Monzon, J.; Chard, A. N.; Guzman, G.; Barrios, E.; Rojop, N.; Arias, K.; Gomez, M.; Paiz, C.; Bolanos, G. A.; Edwards, K. M.; Zielinski Gutierrez, E.; Azziz-Baumgartner, E.; Asturias, E. J.; Santiago, M. L.; Beckham, J. D.; Olson, D. High SARS-CoV-2 Seroprevalence and Rapid Neutralizing Antibody Decline among Agricultural Workers in Rural Guatemala, June 2020-March 2021. *Vaccines (Basel)* **2022**, *10* (7), 1160.
(20) Dinç, H.; Demirci, M.; Özdemir, Y. E.; Sirekbasan, S.; Aktaş, A. N.; Karaali, R.; Tuyji Tok, Y.; Özbey, D.; Akçin, R.; Gareayaghi, N.; Kuşkucu, M. A.; Midilli, K.; Aygün, G.; Sarıbaş, S.; Kocazeybek, B. Anti-SARS-CoV-2 IgG and Neutralizing Antibody Levels in Patients with Past COVID-19 Infection: A Longitudinal Study. *Balkan Med. J.* **2022**, *39* (3), 172−177.
(21) Yang, J.; Chen, C.; Chen, W.; Huang, L.; Fu, Z.; Ye, K.; Lv, L.; Nong, Z.; Zhou, X.; Lu, W.; Zhong, M. Proteomics and metabonomics analyses of Covid-19 complications in patients with pulmonary fibrosis. *Sci. Rep* **2021**, *11* (1), 14601.
(22) Wang, H.; Hui, P.; Uemoto, Y.; Ding, Y.; Yin, Z.; Bao, W. Metabolomic and Proteomic Profiling of Porcine Intestinal Epithelial Cells Infected with Porcine Epidemic Diarrhea Virus. *Int. J. Mol. Sci.* **2023**, *24* (6), 5071.
(23) Shi, J.; Li, Y.; Zhou, X.; Zhang, Q.; Ye, X.; Wu, Z.; Jiang, X.; Yu, H.; Shao, L.; Ai, J. W.; Zhang, H.; Xu, B.; Sun, F.; Zhang, W. Lactate dehydrogenase and susceptibility to deterioration of mild COVID-19 patients: a multicenter nested case-control study. *BMC Med.* **2020**, *18* (1), 168.
(24) Krishnan, S.; Nordqvist, H.; Ambikan, A. T.; Gupta, S.; Sperk, M.; Svensson-Akusjärvi, S.; Mikaeloff, F.; Benfeitas, R.; Saccon, E.; Ponnan, S. M.; Rodriguez, J. E.; Nikouyan, N.; Odeh, A.; Ahlén, G.; Asghar, M.; Sällberg, M.; Vesterbacka, J.; Nowak, P.; Végvári, Á.; Sönnerborg, A.; Treutiger, C. J.; Neogi, U. Metabolic Perturbation Associated With COVID-19 Disease Severity and SARS-CoV-2 Replication. *Mol. Cell Proteomics* **2021**, *20*, 100159.
(25) Ansone, L.; Briviba, M.; Silamikelis, I.; Terentjeva, A.; Perkons, I.; Birzniece, L.; Rovite, V.; Rozentale, B.; Viksna, L.; Kolesova, O.; Klavins, K.; Klovins, J. Amino Acid Metabolism is Significantly Altered at the Time of Admission in Hospital for Severe COVID-19 Patients: Findings from Longitudinal Targeted Metabolomics Analysis. *Microbiol Spectr* **2021**, *9* (3), No. e0033821.
(26) Fan, X.; Liu, Z.; Poulsen, K. L.; Wu, X.; Miyata, T.; Dasarathy, S.; Rotroff, D. M.; Nagy, L. E. Alcohol Consumption Is Associated with Poor Prognosis in Obese Patients with COVID-19: A Mendelian Randomization Study Using UK Biobank. *Nutrients* **2021**, *13* (5), 1592.
(27) Friske, M. M.; Spanagel, R. Chronic alcohol consumption and COVID-19 infection risk: A narrative review. *Alcohol Clin Exp Res. (Hoboken)* **2023**, *47* (4), 629−639.

https://doi.org/10.1021/acsomega.4c04047
ACS Omega 2024, 9, 42757−42765